

Matrix Elements and Few-Body Calculations within the Unitary Correlation Operator Method

R. Roth,* H. Hergert, and P. Papakonstantinou

Institut für Kernphysik, Technische Universität Darmstadt, 64289 Darmstadt, Germany

T. Neff and H. Feldmeier

Gesellschaft für Schwerionenforschung, Planckstr. 1, 64291 Darmstadt, Germany

(Dated: September 10, 2018)

We employ the Unitary Correlation Operator Method (UCOM) to construct correlated, low-momentum matrix elements of realistic nucleon-nucleon interactions. The dominant short-range central and tensor correlations induced by the interaction are included explicitly by a unitary transformation. Using correlated momentum-space matrix elements of the Argonne V18 potential, we show that the unitary transformation eliminates the strong off-diagonal contributions caused by the short-range repulsion and the tensor interaction, and leaves a correlated interaction dominated by low-momentum contributions. We use correlated harmonic oscillator matrix elements as input for no-core shell model calculations for few-nucleon systems. Compared to the bare interaction, the convergence properties are dramatically improved. The bulk of the binding energy can already be obtained in very small model spaces or even with a single Slater determinant. Residual long-range correlations, not treated explicitly by the unitary transformation, can easily be described in model spaces of moderate size allowing for fast convergence. By varying the range of the tensor correlator we are able to map out the Tjon line and can in turn constrain the optimal correlator ranges.

PACS numbers: 21.30.Fe, 21.60.-n, 13.75.Cs

I. INTRODUCTION

One of the prime challenges in modern nuclear structure theory is the description of properties of nuclei across the whole nuclear chart based on realistic nucleon-nucleon interactions. Several modern nucleon-nucleon interactions that reproduce the experimental two-body data with high precision are available, e.g., the Argonne V18 potential [1], the CD Bonn potential [2], or the Nijmegen potentials [3]. The use of these interactions for nuclear structure calculations in a strict *ab initio* fashion is restricted to light isotopes, where Green's Function Monte Carlo [4, 5, 6] or no-core shell model calculations [7, 8, 9] are computationally feasible. These virtually exact solutions of the nuclear many-body problem show that realistic NN-potentials supplemented by a phenomenological three-nucleon force are able to reproduce experimental ground states and excitation spectra of light nuclei. Furthermore, recent developments in chiral perturbation theory provide schemes to construct two- and three-nucleon forces systematically [10, 11].

A major obstacle for *ab initio* nuclear structure calculations are the strong short-range correlations induced by realistic NN-interactions. There are two dominant components: (i) correlations induced by the short-range repulsive core in the central part of the potential and (ii) correlations generated by the strong tensor interaction. It is well known that, in a shell-model language, the description of these correlations requires extremely large model-spaces — the repulsive core and the tensor interaction lead to sizable admixtures of high-lying shells. Simple many-body spaces, which remain tractable for large particle numbers, cannot describe these correlations. In

the extreme case, e.g. in a Hartree-Fock approach, the many-body state is restricted to a single Slater determinant which is not capable of representing these correlations by construction. Therefore, the use of a bare realistic NN-interaction in such a framework has to fail.

There are several recent attempts to tackle this problem. One is the so-called V_{lowk} approach [12, 13], which employs renormalization group techniques to reduce the bare realistic potential to a low-momentum interaction. Effectively, the high-momentum contributions, which are responsible for the admixture of high-lying states, are integrated out leaving an effective low-momentum interaction suitable for small model spaces.

Another approach is the Unitary Correlation Operator Method (UCOM) [14, 15, 16]. Here the short-range central and tensor correlations are explicitly described by a state and basis-independent unitary transformation. Applying the unitary operator of the transformation to uncorrelated many-body states, e.g., the Slater determinant of a Hartree-Fock scheme, leads to a new correlated state which has the dominant short-range correlations built in. Alternatively, the correlation operator can be applied to the Hamiltonian, leading to a phase-shift equivalent correlated interaction V_{UCOM} which is well suited for small low-momentum model spaces. Hence it can be used as an universal input for a variety of many-body methods. The operator form of this correlated interaction resulting for the Argonne V18 (AV18) potential has been used successfully to perform nuclear structure calculations in the framework of Fermionic Molecular Dynamics [16, 17, 18].

In this paper we are going to apply the Unitary Correlation Operator Method to derive correlated two-body matrix elements. They serve as convenient and universal input for a variety of many-body techniques, ranging from Hartree-Fock to shell-model. Following a summary of the formalism of the Unitary Correlation Operator Method in Sec. II,

*Electronic address: robert.roth@physik.tu-darmstadt.de

we derive explicit expressions for correlated matrix elements in Sec. III. Optimal correlation functions for the AV18 potential are constructed in Sec. IV and the properties of the correlated momentum-space matrix elements are discussed in Sec. V. Finally, in Sec. VI, we present results of no-core shell model calculations using correlated oscillator matrix elements, which highlight the effect of the unitary transformation and the properties of the correlated interaction.

II. THE UNITARY CORRELATION OPERATOR METHOD (UCOM)

A. Unitary Correlation Operator

The concept of the Unitary Correlation Operator Method [14, 15, 16] can be summarized as follows: The dominant short-range central and tensor correlations are imprinted into a simple many-body state $|\Psi\rangle$ through a state-independent unitary transformation

$$|\tilde{\Psi}\rangle = C |\Psi\rangle. \quad (1)$$

The unitary correlation operator C describing this transformation is given in an explicit operator form, independent of the particular representation or model space. The correlated many-body state explicitly contains the important short-range correlations generated by the interaction. Even if we start with a simple Slater determinant as uncorrelated state $|\Psi\rangle$ then the correlated state $|\tilde{\Psi}\rangle$ cannot be represented by a single or a superposition of few Slater determinants anymore.

When calculating expectation values or matrix elements of some operator A using correlated states

$$\langle \tilde{\Psi} | A | \tilde{\Psi}' \rangle = \langle \Psi | C^\dagger A C | \Psi' \rangle = \langle \Psi | \tilde{A} | \Psi' \rangle, \quad (2)$$

we can define a correlated operator through the similarity transformation

$$\tilde{A} = C^{-1} A C = C^\dagger A C. \quad (3)$$

Due to the unitarity of C the notions of correlated states and correlated operators are equivalent and we may choose the form that is technically more advantageous.

In the case of the nuclear many-body problem, the unitary correlation operator C has to account for short-range central and tensor correlations as outlined in Sec. I. It is convenient to disentangle these different types of correlations and define the correlation operator as a product of two unitary operators,

$$C = C_\Omega C_r, \quad (4)$$

where C_Ω describes short-range tensor correlations and C_r central correlations. Each of these unitary operators is written as an exponential of a Hermitian two-body generator

$$C_\Omega = \exp\left[-i \sum_{i < j} g_{\Omega, ij}\right], \quad C_r = \exp\left[-i \sum_{i < j} g_{r, ij}\right]. \quad (5)$$

The construction of the generators g_r and g_Ω , which encode the relevant physics of short-range interaction-induced correlations, is crucial.

We start with the generator g_r associated with the short-range central correlations induced by the repulsive core in the central part of the NN-interaction. At small relative distances, the two-body density is strongly suppressed as a result of the repulsive core. Pictorially, the core keeps the nucleons apart from each other so that they reside at larger distances outside the short-range repulsion [14, 16]. These correlations can be imprinted into an uncorrelated many-body state by an unitary distance-dependent shift along the relative coordinate for each particle pair. Such radial shifts are generated by the projection of the relative momentum $\mathbf{q} = \frac{1}{2}[\mathbf{p}_1 - \mathbf{p}_2]$ onto the distance vector $\mathbf{r} = \mathbf{x}_1 - \mathbf{x}_2$ of two particles:

$$q_r = \frac{1}{2} \left[\frac{\mathbf{r}}{r} \cdot \mathbf{q} + \mathbf{q} \cdot \frac{\mathbf{r}}{r} \right]. \quad (6)$$

The distance-dependence of the shift – large shifts at small distances within the core, small or no shifts outside the core – is described by a function $s_{ST}(r)$ for each spin-isospin channel. Their shape depends on the potential under consideration and contains all information on the short-range central correlations. The determination of the $s_{ST}(r)$ is discussed in detail in Sec. IV. The full generator for the central correlations reads

$$g_r = \sum_{S,T} \frac{1}{2} [s_{ST}(r) q_r + q_r s_{ST}(r)] \Pi_{ST}, \quad (7)$$

where Π_{ST} is the projection operator onto two-body spin S and isospin T .

The correlations induced by the tensor part of the interaction are of a more complicated nature. They entangle the spins of the two nucleons with the direction of their relative distance vector \mathbf{r} . Depending on the orientations of the spins, the nucleons are shifted perpendicular to the relative distance vector [15, 16]. Such shifts are generated by the residue of the relative momentum operator after subtracting the radial component

$$\mathbf{q}_\Omega = \mathbf{q} - \frac{\mathbf{r}}{r} q_r = \frac{1}{2r^2} (\mathbf{L} \times \mathbf{r} - \mathbf{r} \times \mathbf{L}). \quad (8)$$

This ‘‘orbital momentum’’, embedded into a tensor operator which encodes the complicated entanglement between spatial and spin degrees of freedom, enters into the generator of the tensor correlations

$$g_\Omega = \sum_T \vartheta_T(r) s_{12}(\mathbf{r}, \mathbf{q}_\Omega) \Pi_{1T} \quad (9)$$

using the general definition

$$s_{12}(\mathbf{a}, \mathbf{b}) = \frac{3}{2} [(\boldsymbol{\sigma}_1 \cdot \mathbf{a})(\boldsymbol{\sigma}_2 \cdot \mathbf{b}) + (\boldsymbol{\sigma}_1 \cdot \mathbf{b})(\boldsymbol{\sigma}_2 \cdot \mathbf{a})] - \frac{1}{2} (\boldsymbol{\sigma}_1 \cdot \boldsymbol{\sigma}_2)(\mathbf{a} \cdot \mathbf{b} + \mathbf{b} \cdot \mathbf{a}). \quad (10)$$

Note, the tensor operator $s_{12}(\mathbf{r}, \mathbf{q}_\Omega)$ entering into the generator g_Ω has the same structure as the standard tensor operator

$s_{12} = s_{12}(\frac{\mathbf{r}}{r}, \frac{\mathbf{r}}{r})$ appearing in the bare potential except for the replacement of one of the relative coordinate vectors by the orbital momentum. Similar to the central correlators the functions $\vartheta_T(r)$ describe the distance dependence of this angular shift for isospin $T = 0$ and $T = 1$. Both, $s_{ST}(r)$ and $\vartheta_T(r)$ have to be in accord with the potential under consideration.

The crucial difference between the Unitary Correlation Operator Method and other schemes using similarity transformations to construct an effective interaction, such as the Lee-Suzuki transformation [19] or the Unitary Model Operator Approach [20], is that our unitary correlation operator is given in an explicit operator form. This enables us to evaluate correlated wave functions or correlated operators analytically as will be shown in the following.

B. Correlated Wave Functions

We consider the effect of the correlation operators on the component of a two-nucleon state that describes the relative motion. The center of mass part is not affected by the unitary correlators because they depend only on relative positions and momenta. For the uncorrelated relative wave function we assume LS -coupled angular momentum eigenstates $|\phi(LS)JM TM_T\rangle$. For the sake of simplicity, the projection quantum numbers M and M_T are omitted in the following.

The central correlator $c_r = \exp(-i g_r)$ [31] affects only the radial part of the state and leaves the angular momentum and spin components unchanged. In coordinate representation it resembles a norm-conserving coordinate transformation [14]

$$\begin{aligned} \langle r | c_r | \phi \rangle &= \frac{R_-(r)}{r} \sqrt{R'_-(r)} \langle R_-(r) | \phi \rangle \\ \langle r | c_r^\dagger | \phi \rangle &= \frac{R_+(r)}{r} \sqrt{R'_+(r)} \langle R_+(r) | \phi \rangle, \end{aligned} \quad (11)$$

where $R_+(r)$ and $R_-(r)$ are mutually inverse, $R_\pm[R_\mp(r)] = r$. These correlation functions are related to the function $s(r)$ in the generator (7) through the integral equation

$$\int_r^{R_\pm(r)} \frac{d\xi}{s(\xi)} = \pm 1. \quad (12)$$

To a certain approximation the following intuitive relation holds $R_\pm(r) \approx r \pm s(r)$. For the sake of brevity we omit the spin and isospin indices of the correlation functions here and in the following.

The action of the tensor correlator c_Ω on LS -coupled two-body states can be evaluated directly [15]. The matrix elements of the tensor operator $s_{12}(\mathbf{r}, \mathbf{q}_\Omega)$ for those states have only off-diagonal contributions

$$\begin{aligned} \langle \phi(J \pm 1, 1)JT | s_{12}(\mathbf{r}, \mathbf{q}_\Omega) | \phi(J \mp 1, 1)JT \rangle \\ = \pm 3i \sqrt{J(J+1)}. \end{aligned} \quad (13)$$

Within a subspace of fixed J one can easily obtain the matrix exponential and thus the matrix elements of the full tensor correlator c_Ω . On this basis we can construct explicit relations for the tensor correlated two-body states.

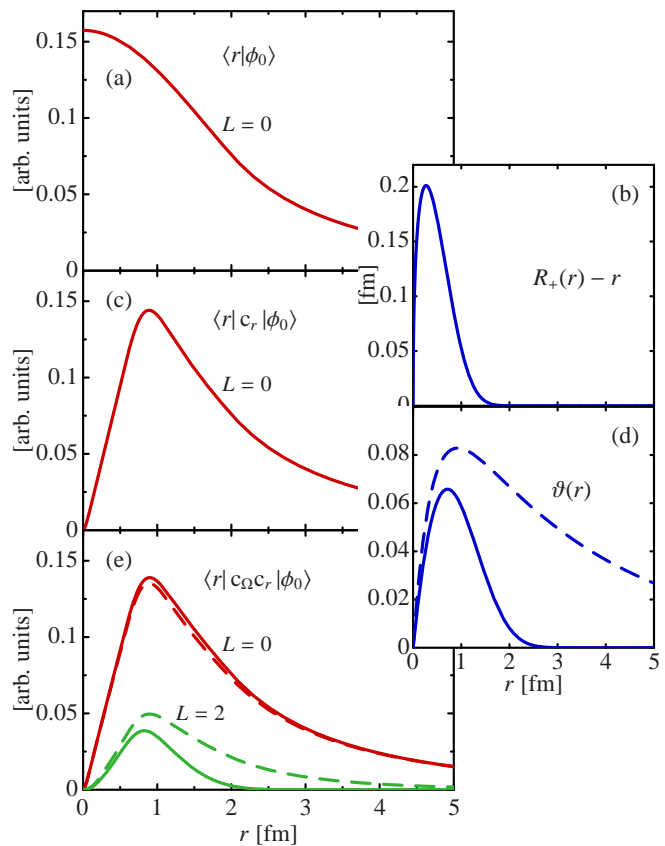


FIG. 1: (Color online) Application of the central and tensor correlators to a deuteron-like two-body wave function. Panels (a), (c), and (e) depict the uncorrelated, the central correlated, and the fully correlated radial wave functions, resp. The panels (b) and (d) show the corresponding central and tensor correlation functions (see text).

States with $L = J$ are invariant under transformation with the tensor correlation operator

$$c_\Omega |\phi(JS)JT\rangle = |\phi(JS)JT\rangle. \quad (14)$$

Only states with $L = J \pm 1$ are susceptible to tensor correlations and transform like

$$\begin{aligned} c_\Omega |\phi(J \pm 1, 1)JT\rangle &= \cos \theta_J(r) |\phi(J \pm 1, 1)JT\rangle \\ &\mp \sin \theta_J(r) |\phi(J \mp 1, 1)JT\rangle \end{aligned} \quad (15)$$

with r being the radial distance operator and

$$\theta_J(r) = 3\sqrt{J(J+1)} \vartheta(r). \quad (16)$$

The tensor correlator admixes a state with $\Delta L = \pm 2$ and changes the radial wave function of both components depending on the tensor correlation function $\vartheta(r)$.

To illustrate the impact of the central and tensor correlation operators on a two-body state, we consider the example of the deuteron. Assume an uncorrelated state $|\phi_0(LS)JT\rangle = |\phi_0(01)10\rangle$ which is a pure S -wave state with the spin-isospin quantum numbers of the deuteron. The radial wave function $\langle r | \phi_0 \rangle$ shall not contain short-range correlations induced by the repulsive core. Fig. 1(a) shows the uncorrelated $L = 0$

radial wave function. Applying the central correlator c_r with the correlation function $R_+(r)$ depicted in panel (b) leads to a wave function which has the short-range central correlations, i.e. the hole at small interparticle distances, built in as depicted in Fig. 1(c). Subsequent application of the tensor correlator c_Ω with the correlation function $\vartheta(r)$ depicted in panel (d) generates the fully correlated wave function shown in Fig. 1(e). As a result of the tensor correlations, the wave function acquires a D -wave admixture whose radial structure depends crucially on the tensor correlation function. In order to represent the long-range D -wave admixture, which is characteristic for the realistic deuteron wave function, a long-ranged tensor correlator is required as indicated by the dashed curve in panels (d) and (e). In the following sections we will argue that only the short-range and state-independent correlations should be described by the correlation operator. The solid curves in panels (d) and (e) correspond to an optimal short-range tensor correlator as will be constructed later-on (see Sec. IV, optimal correlator for $I_\vartheta = 0.09 \text{ fm}^3$).

C. Correlated Operators and Cluster Expansion

The explicit formulation of correlated wave functions for the many-body problem becomes technically increasingly complicated and the equivalent notion of correlated operators proves more convenient.

The similarity transformation (3) of an arbitrary operator A leads to a correlated operator which contains irreducible contributions to all particle numbers. We can formulate a cluster expansion of the correlated operator,

$$\tilde{A} = C^\dagger A C = \tilde{A}^{[1]} + \tilde{A}^{[2]} + \tilde{A}^{[3]} + \dots, \quad (17)$$

where $\tilde{A}^{[n]}$ denotes the irreducible n -body part [14]. When starting with a k -body operator, all irreducible contributions $\tilde{A}^{[n]}$ with $n < k$ vanish. Hence, the unitary transformation of a two-body operator — the NN-interaction for example — yields a correlated operator containing a two-body contribution, a three-body term, etc.

The significance of the higher order terms depends on the range of the central and tensor correlations [14, 15, 16]. If the range of the correlation functions is small compared to the mean interparticle distance, then three-body and higher-order terms of the cluster expansion are negligible. Discarding these higher-order contributions leads to the two-body approximation

$$\tilde{A}^{C2} = \tilde{A}^{[1]} + \tilde{A}^{[2]}. \quad (18)$$

In principle, the higher-order contributions to the cluster expansion can be evaluated systematically [21]. However, for many-body calculations the inclusion of those terms is an extreme challenge.

Therefore, we restrict ourselves to the two-body approximation and choose the correlation functions such that its applicability is ensured. As discussed in detail in Sec. VI we can use exact solutions of the many-body problem, e.g. in the no-core shell model framework, to estimate the size of the omitted higher-order contributions.

D. Correlated Hamiltonian – Central Correlations

In two-body approximation the unitary transformation of any relevant operator with the central correlation operator can be evaluated analytically.

As a comprehensive example we consider a Hamiltonian consisting of kinetic energy and a realistic NN-interaction. For convenience we assume a generic operator form of the interaction

$$v = \sum_p \frac{1}{2} [v_p(r) O_p + O_p v_p(r)] \quad (19)$$

with

$$O_p = \{1, (\boldsymbol{\sigma}_1 \cdot \boldsymbol{\sigma}_2), q_r^2, q_r^2 (\boldsymbol{\sigma}_1 \cdot \boldsymbol{\sigma}_2), \mathbf{L}^2, \mathbf{L}^2 (\boldsymbol{\sigma}_1 \cdot \boldsymbol{\sigma}_2), (\mathbf{L} \cdot \mathbf{S}), s_{12}(\frac{\mathbf{r}}{r}, \frac{\mathbf{r}}{r}), s_{12}(\mathbf{L}, \mathbf{L})\} \otimes \{1, (\boldsymbol{\tau}_1 \cdot \boldsymbol{\tau}_2)\}. \quad (20)$$

In order to accommodate momentum dependent terms, as they appear, e.g., in the Nijmegen [3] or Bonn A/B potentials [22], we have chosen an explicitly symmetrized form. Notice, that any quadratic momentum dependence can be expressed by the q_r^2 and \mathbf{L}^2 terms contained in (19). For simplicity, charge dependent terms are not explicitly discussed here. Nevertheless, they will be included in Sec. VI.

For the formulation of the correlated Hamiltonian in two-body approximation, it is sufficient to consider the Hamiltonian for a two-nucleon system given by

$$h = T + v = t_{cm} + t_r + t_\Omega + v, \quad (21)$$

where we have decomposed the kinetic energy operator T into a center of mass contribution t_{cm} and a relative contribution which in turn is written as a sum of a radial and an angular part

$$t_r = \frac{1}{2\mu} q_r^2, \quad t_\Omega = \frac{1}{2\mu} \frac{\mathbf{L}^2}{r^2}. \quad (22)$$

Applying the central correlator c_r in two-body space leads to a correlated Hamiltonian consisting of the bare kinetic energy T and two-body contributions for the correlated radial and angular kinetic energy, $\tilde{t}_r^{[2]}$ and $\tilde{t}_\Omega^{[2]}$, resp., as well as the correlated two-body interaction $\tilde{v}^{[2]}$

$$c_r^\dagger h c_r = T + \tilde{t}_r^{[2]} + \tilde{t}_\Omega^{[2]} + \tilde{v}^{[2]}. \quad (23)$$

The explicit operator form of the correlated terms can be derived from a few basic identities. The similarity transformation for the relative distance operator r results in the operator-valued function $R_+(r)$

$$c_r^\dagger r c_r = R_+(r). \quad (24)$$

The unitarity $c_r^\dagger = c_r^{-1}$ implies that an arbitrary function of r transforms as

$$c_r^\dagger f(r) c_r = f(c_r^\dagger r c_r) = f(R_+(r)). \quad (25)$$

The interpretation of the unitary transformation in terms of a norm-conserving coordinate transformation $r \mapsto R_+(r)$ is evident. For the radial momentum operator q_r one finds the following correlated form [14]

$$c_r^\dagger q_r c_r = \frac{1}{\sqrt{R'_+(r)}} q_r \frac{1}{\sqrt{R'_+(r)}}. \quad (26)$$

With this, we obtain the following expression for the square of the radial momentum, which enters into the radial part of the kinetic energy

$$c_r^\dagger q_r^2 c_r = \frac{1}{2} \left[\frac{1}{R'_+(r)^2} q_r^2 + q_r^2 \frac{1}{R'_+(r)^2} \right] + w(r) \quad (27)$$

with an additional local term depending only on the correlation function $R_+(r)$

$$w(r) = \frac{7R''_+(r)^2}{4R'_+(r)^4} - \frac{R''_+(r)}{2R'_+(r)^3}. \quad (28)$$

All other basic operators, such as \mathbf{L}^2 , $(\mathbf{L} \cdot \mathbf{S})$, s_{12} etc. commute with the correlation operator c_r and are therefore invariant.

Based on these elementary relations we can explicitly construct the two-body contributions to the correlated kinetic energy. For the radial part we obtain using (27)

$$\begin{aligned} \tilde{t}_r^{[2]} &= c_r^\dagger t_r c_r - t_r \\ &= \frac{1}{2} \left(\frac{1}{2\mu_r(r)} q_r^2 + q_r^2 \frac{1}{2\mu_r(r)} \right) + \frac{1}{2\mu} w(r) \end{aligned} \quad (29)$$

with a distance-dependent effective mass term

$$\frac{1}{2\mu_r(r)} = \frac{1}{2\mu} \left(\frac{1}{R'_+(r)^2} - 1 \right). \quad (30)$$

The two-body contribution to the correlated angular part of the kinetic energy involves only the basic relation (26) and reads

$$\tilde{t}_\Omega^{[2]} = c_r^\dagger t_\Omega c_r - t_\Omega = \frac{1}{2\mu_\Omega(r)} \frac{\mathbf{L}^2}{r^2} \quad (31)$$

with a distance-dependent angular effective mass term

$$\frac{1}{2\mu_\Omega(r)} = \frac{1}{2\mu} \left(\frac{r^2}{R_+(r)^2} - 1 \right). \quad (32)$$

The momentum dependent terms of the NN-interaction (19) transform in a similar manner like the kinetic energy. Using (26) and (27) we obtain

$$\begin{aligned} c_r^\dagger \frac{1}{2} \left(q_r^2 v(r) + v(r) q_r^2 \right) c_r &= \\ &= \frac{1}{2} \left(\frac{v(R_+(r))}{R'_+(r)^2} q_r^2 + q_r^2 \frac{v(R_+(r))}{R'_+(r)^2} \right) \\ &+ v(R_+(r)) w(r) - v'(R_+(r)) \frac{R''_+(r)}{R'_+(r)^2}. \end{aligned} \quad (33)$$

For all other terms of the NN-interaction (19) the commutator relations $[q_r, O_p] = [r, O_p] = 0$ are fulfilled and the similarity transformation with the central correlator reduces to

$$c_r^\dagger v(r) O_p c_r = v(R_+(r)) O_p. \quad (34)$$

Many of the other relevant operators, e.g. the quadratic radius or transition operators, can be transformed just as easily.

E. Correlated Hamiltonian – Tensor Correlations

The transformation of the Hamiltonian with the tensor correlation operator c_Ω is more involved. In general, it can be evaluated via the Baker-Campbell-Hausdorff expansion

$$c_\Omega^\dagger A c_\Omega = A + i[g_\Omega, A] + \frac{i^2}{2}[g_\Omega, [g_\Omega, A]] + \dots \quad (35)$$

Evaluation of the iterated commutators in some cases results in a termination of the series expansion. A trivial case is the distance operator r which commutes with the tensor generator g_Ω and is thus invariant under the transformation

$$c_\Omega^\dagger r c_\Omega = r. \quad (36)$$

For the radial momentum operator q_r , the expansion (35) terminates after the first order commutators and we obtain the simple expression

$$c_\Omega^\dagger q_r c_\Omega = q_r - \vartheta'(r) s_{12}(\mathbf{r}, \mathbf{q}_\Omega). \quad (37)$$

Likewise, we find for the tensor correlated quadratic radial momentum operator

$$\begin{aligned} c_\Omega^\dagger q_r^2 c_\Omega &= q_r^2 - [\vartheta'(r) q_r + q_r \vartheta'(r)] s_{12}(\mathbf{r}, \mathbf{q}_\Omega) \\ &+ [\vartheta'(r) s_{12}(\mathbf{r}, \mathbf{q}_\Omega)]^2, \end{aligned} \quad (38)$$

where $s_{12}(\mathbf{r}, \mathbf{q}_\Omega)^2 = 9[\mathbf{S}^2 + 3(\mathbf{L} \cdot \mathbf{S}) + (\mathbf{L} \cdot \mathbf{S})^2]$. For all other operators of the interaction (19), that involve angular degrees of freedom, the Baker-Campbell-Hausdorff series does not terminate. Through the commutators additional tensor operators are generated. For example, the relevant first order commutators are

$$\begin{aligned} [g_\Omega, s_{12}(\frac{\mathbf{r}}{r}, \frac{\mathbf{r}}{r})] &= i\vartheta(r)[-24\Pi_1 - 18(\mathbf{L} \cdot \mathbf{S}) + 3s_{12}(\frac{\mathbf{r}}{r}, \frac{\mathbf{r}}{r})] \\ [g_\Omega, (\mathbf{L} \cdot \mathbf{S})] &= i\vartheta(r)[-5s_{12}(\mathbf{q}_\Omega, \mathbf{q}_\Omega)] \\ [g_\Omega, \mathbf{L}^2] &= i\vartheta(r)[2\bar{s}_{12}(\mathbf{q}_\Omega, \mathbf{q}_\Omega)] \\ [g_\Omega, s_{12}(\mathbf{L}, \mathbf{L})] &= i\vartheta(r)[7\bar{s}_{12}(\mathbf{q}_\Omega, \mathbf{q}_\Omega)], \end{aligned} \quad (39)$$

where

$$\bar{s}_{12}(\mathbf{q}_\Omega, \mathbf{q}_\Omega) = 2r^2 s_{12}(\mathbf{q}_\Omega, \mathbf{q}_\Omega) + s_{12}(\mathbf{L}, \mathbf{L}) - \frac{1}{2} s_{12}(\frac{\mathbf{r}}{r}, \frac{\mathbf{r}}{r}). \quad (40)$$

The next order generates higher powers of the orbital angular momentum operator, e.g. an $\mathbf{L}^2(\mathbf{L} \cdot \mathbf{S})$ term, in addition. The resulting accumulation of new operators enforces a truncation of the Baker-Campbell-Hausdorff expansion at some finite order for the operator representation [16]. The basis representation introduced in Sec. III does not require this approximation.

F. Correlated Interaction – V_{UCOM}

Subtracting the uncorrelated kinetic energy operator from the central and tensor correlated Hamiltonian in two-body

space defines the correlated interaction v_{UCOM} in two-body approximation:

$$v_{\text{UCOM}} = c_r^\dagger c_\Omega^\dagger h c_\Omega c_r - T. \quad (41)$$

If we start from a realistic interaction which is given in an operator representation, e.g. the AV18 potential, then the correlated interaction also has a closed operator representation

$$v_{\text{UCOM}} = \sum_p \frac{1}{2} [\tilde{v}_p(r) \tilde{O}_p + \tilde{O}_p \tilde{v}_p(r)], \quad (42)$$

where

$$\begin{aligned} \tilde{O}_p = \{ & 1, (\boldsymbol{\sigma}_1 \cdot \boldsymbol{\sigma}_2), q_r^2, q_r^2 (\boldsymbol{\sigma}_1 \cdot \boldsymbol{\sigma}_2), \mathbf{L}^2, \mathbf{L}^2 (\boldsymbol{\sigma}_1 \cdot \boldsymbol{\sigma}_2), \\ & (\mathbf{L} \cdot \mathbf{S}), s_{12}(\frac{\mathbf{r}}{r}, \frac{\mathbf{r}}{r}), s_{12}(\mathbf{L}, \mathbf{L}), \\ & \bar{s}_{12}(\mathbf{q}_\Omega, \mathbf{q}_\Omega), q_r s_{12}(\mathbf{r}, \mathbf{q}_\Omega), \mathbf{L}^2 (\mathbf{L} \cdot \mathbf{S}), \\ & \mathbf{L}^2 \bar{s}_{12}(\mathbf{q}_\Omega, \mathbf{q}_\Omega), \dots \} \otimes \{1, (\boldsymbol{\tau}_1 \cdot \boldsymbol{\tau}_2)\}. \end{aligned} \quad (43)$$

The dots indicate that higher-order contributions of the Baker-Campbell-Hausdorff expansion for the tensor transformation have been omitted. The terms shown above result from a truncation of the expansion (35) after the third order in g_Ω . For most applications the inclusion of these terms is sufficient [16].

The existence of an operator representation of v_{UCOM} is essential for many-body models which are not based on a simple oscillator or plane-wave basis. One example is the Fermionic Molecular Dynamics model [23, 24] which uses a non-orthogonal Gaussian basis and does not easily allow for a partial wave decomposition of the relative two-body states. Nevertheless, it is possible to evaluate the two-body matrix elements of v_{UCOM} analytically, which facilitates efficient computations with this extremely versatile basis [16, 17, 18].

As we have emphasized already, the operators of *all observables* have to be transformed *consistently*. The unitary transformation of observables like quadratic radii, densities, momentum distributions, or transition matrix elements is straightforward given the toolbox acquired for the transformation of the Hamiltonian. The Unitary Correlation Operator Method owes this simplicity to the explicit state and representation-independent form of the correlation operators. In contrast, in many other approaches for the construction of an effective interaction, e.g. the Lee-Suzuki transformation [7, 9, 19] or the $V_{\text{low}k}$ renormalization group method [12], the consistent derivation of effective quantities other than the interaction is a complicated and rarely addressed problem [25].

An important feature of v_{UCOM} results from the finite range of the correlation functions $s_{ST}(r)$ and $\vartheta_T(r)$ entering into the generators. Since the correlation functions vanish at large distances — i.e., the correlation operator acts as a unit operator at large r — asymptotic properties of a two-body wave function are preserved. This implies that v_{UCOM} is by construction *phase-shift equivalent* to the original NN-interaction. The unitary transformation can, therefore, be viewed as a way to construct an infinite manifold of realistic potentials, which all give identical phase-shifts.

It is interesting to observe in which way the unitary transformation changes the operator of the interaction while preserving the phase-shifts. The central correlator reduces the short-range repulsion in the local part of the interaction and, at the same time, creates a non-local repulsion through the momentum-dependent terms. The tensor correlator removes some strength from the local tensor interaction and creates additional central contributions as well as new non-local tensor terms. Hence, the unitary transformation exploits the freedom to redistribute strength between local and non-local parts of the potential without changing the phase-shifts. The non-local tensor terms establish an interesting connection to the CD Bonn potential, which among the realistic potentials is the only one including non-local tensor contributions [26].

III. CORRELATED TWO-BODY MATRIX ELEMENTS

Having introduced the basic formalism of the Unitary Correlation Operator Method, we can now derive two-body matrix elements of the correlated interaction v_{UCOM} . We consider relative LS -coupled states of the form $|n(LS)JM T M_T\rangle$, with a generic radial quantum number n , relative orbital angular momentum L , spin S , total angular momentum J , and isospin T . The matrix elements of v_{UCOM} thus read

$$\begin{aligned} & \langle n(LS)JM T M_T | v_{\text{UCOM}} | n'(L'S)JM T M_T \rangle \\ & = \langle n(LS)JM T M_T | c_r^\dagger c_\Omega^\dagger h c_\Omega c_r - T | n'(L'S)JM T M_T \rangle. \end{aligned} \quad (44)$$

The center of mass part of the two-body states is irrelevant for the unitary transformation, since the correlation operator only acts on the relative degrees of freedom of the two-body states. In the following derivations the projection quantum numbers M and M_T are omitted for simplicity. The formal framework discussed in the following is completely independent of the particular choice of basis, only the angular momentum structure is relevant.

The Unitary Correlation Operator Method offers different ways to compute these matrix elements. If we assume a NN-interaction of the form (19), then we can use the operator representation (42) of v_{UCOM} and evaluate the matrix elements directly. This approach is computationally quite efficient. If one expands the radial dependencies of the individual operator channels in a sum of Gauss functions, all radial integrals can be calculated analytically. The matrix elements of the additional tensor operators contained in v_{UCOM} can be given in closed form as well. However, this direct approach relies on the truncation of the Baker-Campbell-Hausdorff expansion (35) employed to evaluate the tensor correlation.

In order to avoid this approximation for the tensor transformation we apply the tensor correlators to the two-body states and make use of the exact expressions (14) and (15). The central correlators will be applied to the operator as before, since a simple and exact expression for the central correlated Hamiltonian exists (cf. Sec. IID). We formally interchange

the ordering of the correlations operators using the identity

$$\begin{aligned} c_r^\dagger c_\Omega^\dagger h c_\Omega c_r &= (c_r^\dagger c_\Omega^\dagger c_r) c_r^\dagger h c_r (c_r^\dagger c_\Omega c_r) \\ &= \tilde{c}_\Omega^\dagger c_r^\dagger h c_r \tilde{c}_\Omega \end{aligned} \quad (45)$$

with the ‘‘centrally correlated’’ tensor correlation operator

$$\tilde{c}_\Omega = c_r^\dagger c_\Omega c_r = \exp[-i\vartheta(R_+(r)) s_{12}(\mathbf{r}, \mathbf{q}_\Omega)]. \quad (46)$$

The central correlator commutes with $s_{12}(\mathbf{r}, \mathbf{q}_\Omega)$ and transforms therefore only $\vartheta(r)$, see Eq. (25). The tensor correlator \tilde{c}_Ω acts on LS -coupled two-body states with $L = J$ like the identity operator (cf. Sec. II B)

$$\tilde{c}_\Omega |n(JS)JT\rangle = |n(JS)JT\rangle. \quad (47)$$

For states with $L = J \pm 1$ we have the simple relation

$$\begin{aligned} \tilde{c}_\Omega |n(J \mp 1, 1)JT\rangle &= \cos \tilde{\theta}_J(r) |n(J \mp 1, 1)JT\rangle \\ &\pm \sin \tilde{\theta}_J(r) |n(J \pm 1, 1)JT\rangle, \end{aligned} \quad (48)$$

where

$$\tilde{\theta}_J(r) = 3\sqrt{J(J+1)}\vartheta(R_+(r)). \quad (49)$$

Using these relations we can calculate the correlated two-body matrix elements exactly.

A. Interactions in operator representation

We first consider a bare potential given in the generic operator representation (19) and derive the correlated matrix elements for the local contributions of the form $v(\mathbf{r})\mathbf{O}$ with $[\mathbf{r}, \mathbf{O}] = [\mathbf{q}_r, \mathbf{O}] = 0$, which includes all operators of the set (20) except for the q_r^2 terms.

The matrix elements for $L = L' = J$ are not affected by the tensor correlations, only the central correlators act according to (34). In coordinate representation we obtain

$$\begin{aligned} \langle n(JS)JT | c_r^\dagger c_\Omega^\dagger v(\mathbf{r})\mathbf{O} c_\Omega c_r | n'(JS)JT \rangle &= \\ = \int d\mathbf{r} u_{n,J}^*(r) u_{n',J}(r) \tilde{v}(r) \langle (JS)JT | \mathbf{O} | (JS)JT \rangle, \end{aligned} \quad (50)$$

where $\tilde{v}(r) = v(R_+(r))$ is the transformed radial dependence of the potential. The $u_{n,L}(r) = r\phi_{n,L}(r)$ are the radial relative wave functions of the oscillator basis or any other basis under consideration. For the diagonal matrix elements with $L = L' = J \mp 1$ we get

$$\begin{aligned} \langle n(J \mp 1, 1)JT | c_r^\dagger c_\Omega^\dagger v(\mathbf{r})\mathbf{O} c_\Omega c_r | n'(J \mp 1, 1)JT \rangle &= \\ = \int d\mathbf{r} u_{n,J \mp 1}^*(r) u_{n',J \mp 1}(r) \tilde{v}(r) & \\ \times [\langle (J \mp 1, 1)JT | \mathbf{O} | (J \mp 1, 1)JT \rangle \cos^2 \tilde{\theta}_J(r) & \\ + \langle (J \pm 1, 1)JT | \mathbf{O} | (J \pm 1, 1)JT \rangle \sin^2 \tilde{\theta}_J(r) & \\ \pm \langle (J \mp 1, 1)JT | \mathbf{O} | (J \pm 1, 1)JT \rangle 2 \cos \tilde{\theta}_J(r) \sin \tilde{\theta}_J(r)] & \end{aligned} \quad (51)$$

with $\tilde{\theta}_J(r) = \theta_J(R_+(r))$. Finally, the off-diagonal matrix elements for $L = J \mp 1$ and $L' = J \pm 1$ read

$$\begin{aligned} \langle n(J \mp 1, 1)JT | c_r^\dagger c_\Omega^\dagger v(\mathbf{r})\mathbf{O} c_\Omega c_r | n'(J \pm 1, 1)JT \rangle &= \\ = \int d\mathbf{r} u_{n,J \mp 1}^*(r) u_{n',J \pm 1}(r) \tilde{v}(r) & \\ \times [\langle (J \mp 1, 1)JT | \mathbf{O} | (J \pm 1, 1)JT \rangle \cos^2 \tilde{\theta}_J(r) & \\ - \langle (J \pm 1, 1)JT | \mathbf{O} | (J \mp 1, 1)JT \rangle \sin^2 \tilde{\theta}_J(r) & \\ \mp \langle (J \mp 1, 1)JT | \mathbf{O} | (J \mp 1, 1)JT \rangle \cos \tilde{\theta}_J(r) \sin \tilde{\theta}_J(r) & \\ \pm \langle (J \pm 1, 1)JT | \mathbf{O} | (J \pm 1, 1)JT \rangle \sin \tilde{\theta}_J(r) \cos \tilde{\theta}_J(r)] & \end{aligned} \quad (52)$$

Apart from the integration involving the radial wave functions, the matrix elements of the operators \mathbf{O} in LS -coupled angular momentum states are required. Only for the standard tensor operator $\mathbf{O} = s_{12}(\frac{\mathbf{r}}{r}, \frac{\mathbf{r}}{r})$ the off-diagonal terms on the right hand side of Eqs. (51) and (52) contribute. For all other operators in (20) the off-diagonal matrix elements vanish, and the above equations simplify significantly.

The effect of the tensor correlator is clearly visible in the structure of the correlated matrix elements (51) and (52). It admixes components with $\Delta L = \pm 2$ to the states. Therefore, the correlated matrix element consists of a linear combination of diagonal and off-diagonal matrix elements $\langle (LS)JT | \mathbf{O} | (L'S)JT \rangle$. In this way even simple operators, like \mathbf{L}^2 or $(\mathbf{L} \cdot \mathbf{S})$ acquire non-vanishing off-diagonal *correlated* matrix elements (52).

The momentum dependent terms of the potential (19) allow for an exact evaluation of the similarity transformation on the operator level. For the tensor correlated form of the operator

$$v_{qr} = \frac{1}{2} [v(\mathbf{r})q_r^2 + q_r^2 v(\mathbf{r})] \quad (53)$$

we obtain

$$\begin{aligned} c_\Omega^\dagger v_{qr} c_\Omega &= \frac{1}{2} [v(\mathbf{r})q_r^2 + q_r^2 v(\mathbf{r})] + v(\mathbf{r})[\vartheta'(r)s_{12}(\mathbf{r}, \mathbf{q}_\Omega)]^2 \\ &- [v(\mathbf{r})\vartheta'(r)q_r + q_r\vartheta'(r)v(\mathbf{r})]s_{12}(\mathbf{r}, \mathbf{q}_\Omega) \end{aligned} \quad (54)$$

by using Eq. (38). Subsequent inclusion of the central correlations leads to the following expression for the diagonal matrix elements with $L = L' = J$ in coordinate representation:

$$\begin{aligned} \langle n(JS)JT | c_r^\dagger c_\Omega^\dagger v_{qr} c_\Omega c_r | n'(JS)JT \rangle &= \\ = \int d\mathbf{r} \left\{ u_{n,J}^*(r) u_{n',J}(r) \left[\tilde{v}(r) w(r) - \tilde{v}'(r) \frac{R_+''(r)}{R_+'(r)^2} \right] \right. & \\ \left. - \frac{1}{2} [u_{n,J}^*(r) u_{n',J}''(r) + u_{n,J}''(r) u_{n',J}(r)] \frac{\tilde{v}(r)}{R_+'(r)^2} \right\}, \end{aligned} \quad (55)$$

where $\tilde{v}'(r) = v'(R_+(r))$. As before, the tensor correlator does not affect these matrix elements and only the central correlations lead to a modification. For the diagonal matrix elements with $L = L' = J \mp 1$ the tensor terms contribute and

we obtain

$$\begin{aligned}
& \langle n(J \mp 1, 1)JT | c_r^\dagger c_\Omega^\dagger v_{qr} c_\Omega c_r | n'(J \mp 1, 1)JT \rangle \\
&= \int dr \left\{ u_{n, J \mp 1}^*(r) u_{n', J \mp 1}(r) \left[\tilde{v}(r) w(r) + \tilde{v}(r) \tilde{\theta}'_J(r)^2 \right. \right. \\
&\quad \left. \left. - \tilde{v}'(r) \frac{R_+''(r)}{R_+(r)^2} \right] - \frac{1}{2} [u_{n, J \mp 1}^*(r) u_{n', J \mp 1}''(r) \right. \\
&\quad \left. + u_{n, J \mp 1}''^*(r) u_{n', J \mp 1}(r)] \frac{\tilde{v}(r)}{R_+(r)^2} \right\} \quad (56)
\end{aligned}$$

with $\tilde{\theta}'_J(r) = \theta'_J(R_+(r))$. Likewise, we find

$$\begin{aligned}
& \langle n(J \mp 1, 1)JT | c_r^\dagger c_\Omega^\dagger v_{qr} c_\Omega c_r | n'(J \pm 1, 1)JT \rangle \\
&= \pm \int dr \left[u_{n, J \mp 1}^*(r) u'_{n', J \pm 1}(r) - u'_{n, J \mp 1}^*(r) u_{n', J \pm 1}(r) \right] \\
&\quad \times \frac{\tilde{v}(r) \tilde{\theta}'_J(r)}{R_+(r)} \quad (57)
\end{aligned}$$

for the off-diagonal matrix elements with $L = J \mp 1$ and $L' = J \pm 1$.

The matrix elements for the correlated radial and angular kinetic energy can be constructed as special cases of the interaction matrix elements discussed above. By setting $v(r) = 1/(2\mu_r(r))$ in Eqs. (55) to (57) we obtain the matrix elements for the effective mass part of the correlated radial kinetic energy (29). The matrix elements of the additional local potential in (29) and the angular kinetic energy (31) follow directly from Eqs. (50) to (52).

B. Interactions in partial-wave representation

So far we have discussed interactions given in a closed operator representation of the form (19). However, many modern interactions, e.g., the CD Bonn potential or recent chiral potentials, are defined using a non-local partial-wave representation. This makes it difficult to employ them within many-body models which do not allow for a partial-wave expansion of the two-body states [16]. Nevertheless, the calculation of central and tensor correlated matrix elements of the form (44) is straightforward for those interactions.

Consider a general non-local NN-potential in partial-wave representation. For simplicity we assume the potential given in a generic coordinate space representation

$$\begin{aligned}
v &= \int dr r^2 \int dr' r'^2 \sum_{L, L', S, J, T} \\
& |r(LS)JT \rangle v_{LL'SJT}(r, r') \langle r'(L'S)JT | , \quad (58)
\end{aligned}$$

where M and M_T have been omitted for brevity. Interactions given in momentum space can be easily transformed into this representation.

For the construction of the correlated matrix elements we only need the expressions for correlated two-body states used

in the previous section. For $L = L' = J$ the tensor correlations are not active and we obtain

$$\begin{aligned}
& \langle n(JS)JT | c_r^\dagger c_\Omega^\dagger v c_\Omega c_r | n'(JS)JT \rangle \\
&= \int dr r \mathcal{R}_+(r) \int dr' r' \mathcal{R}_+(r') u_{n, J}^*(r) u_{n', J}(r') \\
&\quad \times \tilde{v}_{J, J, S, J, T}(r, r') , \quad (59)
\end{aligned}$$

where $\tilde{v}_{LL'SJT}(r, r') = v_{LL'SJT}(R_+(r), R_+(r'))$. Due to the non-local character with respect to the relative coordinate, the metric factors $\mathcal{R}_+(r) = \sqrt{R_+'(r)} R_+(r)/r$ resulting from the transformation of the radial wave function remain. For the diagonal matrix elements $L = L' = J \mp 1$ of the non-local interaction (58) we obtain

$$\begin{aligned}
& \langle n(J \mp 1, 1)JT | c_r^\dagger c_\Omega^\dagger v c_\Omega c_r | n'(J \mp 1, 1)JT \rangle = \\
&= \int dr r \mathcal{R}_+(r) \int dr' r' \mathcal{R}_+(r') u_{n, J \mp 1}^*(r) u_{n', J \mp 1}(r') \\
&\quad \times \left[\tilde{v}_{J \mp 1, J \mp 1, 1, J, T}(r, r') \cos \tilde{\theta}_J(r) \cos \tilde{\theta}_J(r') \right. \\
&\quad + \tilde{v}_{J \pm 1, J \pm 1, 1, J, T}(r, r') \sin \tilde{\theta}_J(r) \sin \tilde{\theta}_J(r') \\
&\quad \pm \tilde{v}_{J \mp 1, J \pm 1, 1, J, T}(r, r') \cos \tilde{\theta}_J(r) \sin \tilde{\theta}_J(r') \\
&\quad \left. \pm \tilde{v}_{J \pm 1, J \mp 1, 1, J, T}(r, r') \sin \tilde{\theta}_J(r) \cos \tilde{\theta}_J(r') \right] \quad (60)
\end{aligned}$$

with $\tilde{\theta}_J(r) = \theta_J(R_+(r))$. Finally, the off-diagonal matrix elements with $L = J \mp 1$ and $L' = J \pm 1$ read

$$\begin{aligned}
& \langle n(J \mp 1, 1)JT | c_r^\dagger c_\Omega^\dagger v c_\Omega c_r | n'(J \pm 1, 1)JT \rangle = \\
&= \int dr r \mathcal{R}_+(r) \int dr' r' \mathcal{R}_+(r') u_{n, J \mp 1}^*(r) u_{n', J \pm 1}(r') \\
&\quad \times \left[\tilde{v}_{J \mp 1, J \pm 1, 1, J, T}(r, r') \cos \tilde{\theta}_J(r) \cos \tilde{\theta}_J(r') \right. \\
&\quad - \tilde{v}_{J \pm 1, J \mp 1, 1, J, T}(r, r') \sin \tilde{\theta}_J(r) \sin \tilde{\theta}_J(r') \\
&\quad \mp \tilde{v}_{J \mp 1, J \mp 1, 1, J, T}(r, r') \cos \tilde{\theta}_J(r) \sin \tilde{\theta}_J(r') \\
&\quad \left. \pm \tilde{v}_{J \pm 1, J \pm 1, 1, J, T}(r, r') \sin \tilde{\theta}_J(r) \cos \tilde{\theta}_J(r') \right] . \quad (61)
\end{aligned}$$

For local interactions $v_{LL'SJT}(r, r') = v_{LL'SJT}^{\text{loc}}(r) \delta(r - r')/(r'r)$ the metric factors $\mathcal{R}_+(r)$ can be eliminated and the above equations simplify substantially. For technical reasons we use these expression also for the calculations with the AV18 potential discussed in the following.

IV. OPTIMAL CORRELATION FUNCTIONS

The Unitary Correlation Operator Method encapsulates the physics of short-range central and tensor correlations in the set of correlation functions $s(r)$ and $\vartheta(r)$. In this section, we discuss a scheme to determine these correlation functions for a given NN-potential. One important task is to isolate the short-range state-independent correlations from residual long-range correlations that should not be described by the unitary transformation but by the many-body state.

The most convenient procedure to fix the correlation functions is based on an energy minimization in the two-body system [15]. For each combination of spin S and isospin T we compute the correlated energy expectation value using a two-body trial state with the lowest possible orbital angular momentum L . The uncorrelated radial wave function should not contain any of the short-range correlations, i.e., it should resemble the short-range behavior of a non-interacting system. In the following we will use a free zero-energy scattering solution $\phi_L(r) \propto r^L$. One could just as well use harmonic oscillator wave functions, the difference in the resulting correlation functions is marginal.

The correlation functions are represented by parametrizations with typically three variational parameters. The long-range part is generally well-described by a double-exponential decay with variable range. For the short-range behavior, several different parametrizations have been compared. For the AV18 potential, the following two parametrizations have proven most appropriate:

$$\begin{aligned} R_+^I(r) &= r + \alpha (r/\beta)^\eta \exp[-\exp(r/\beta)] , \\ R_+^{II}(r) &= r + \alpha [1 - \exp(-r/\gamma)] \exp[-\exp(r/\beta)] . \end{aligned} \quad (62)$$

Which of these parametrizations is best suited for a particular channel will be decided on the basis of the minimal energy alone. Note that rather than $s(r)$, we directly parametrize the function $R_+(r)$, which enters into the expressions for correlated operators and matrix elements. For the tensor correlation functions the following parametrization is used

$$\vartheta(r) = \alpha [1 - \exp(-r/\gamma)] \exp[-\exp(r/\beta)] . \quad (63)$$

The $S = 0$ channels are only affected by the central correlators. Their parameters are determined from the energy minimization within the lowest possible orbital angular momentum state, i.e. $L = 1$ for $T = 0$ and $L = 0$ for $T = 1$, resp.,

$$\begin{aligned} E_{00} &= \langle \phi_1(10)10 | c_r^\dagger h c_r | \phi_1(10)10 \rangle , \\ E_{01} &= \langle \phi_0(00)01 | c_r^\dagger h c_r | \phi_0(00)01 \rangle . \end{aligned} \quad (64)$$

For $S = 0, T = 1$ the minimization of E_{01} by variation of the parameters of the central correlation function is straightforward. The resulting parameters are summarized in Table I. For $S = 0, T = 0$ the potential is purely repulsive and, therefore, the energy minimization, for a negligible gain in energy, leads to central correlation functions of very long range. In order to avoid this pathology we employ a constraint on the strength of the correlation function defined through

$$I_{R_+} = \int dr r^2 (R_+(r) - r) . \quad (65)$$

The value of this constraint on the central correlation function for the $S = 0, T = 0$ channel is fixed to $I_{R_+} = 0.1\text{fm}^4$ in accord with the typical values in the other channels.

For $S = 1$ the tensor correlations are active as well and we determine the parameters of the central and the tensor correlation functions simultaneously. For $T = 0$ the energy is

S	T	Param.	α [fm]	β [fm]	γ [fm]	η
0	0	II	0.7971	1.2638	0.4621	—
0	1	I	1.3793	0.8853	—	0.3724
1	0	I	1.3265	0.8342	—	0.4471
1	1	II	0.5665	1.3888	0.1786	—

TABLE I: Parameters of the central correlation functions $R_+(r)$ for the AV18 potential obtained from two-body energy minimization.

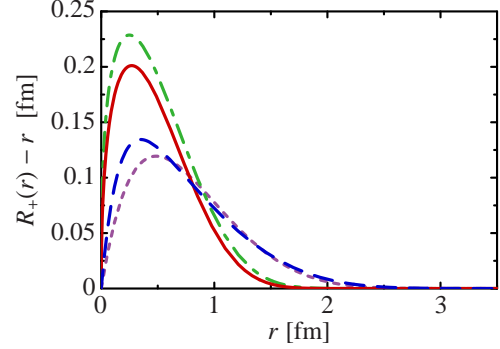


FIG. 2: (Color online) Optimal central correlation functions $R_+(r) - r$ for the AV18 potential according to the parameters given in Tab. I. The curves correspond to the different spin-isospin channels: $(S, T) = (0, 1)$ (---), $(1, 0)$ (—), $(0, 0)$ (····), $(1, 1)$ (-·-·)

defined by the matrix element with $L = 0$ states

$$E_{10} = \langle \phi_0(01)10 | c_r^\dagger c_\Omega^\dagger h c_\Omega c_r | \phi_0(01)10 \rangle . \quad (66)$$

For $T = 1$ the lowest possible orbital angular momentum is $L = 1$. From angular momentum coupling we obtain 0, 1, and 2 as possible values for J . Therefore, we define the energy functional which is used in the minimization procedure as the sum over all three possibilities with relative weights given by $2J + 1$

$$\begin{aligned} E_{11} &= \frac{1}{9} \langle \phi_1(11)01 | c_r^\dagger h c_r | \phi_1(11)01 \rangle \\ &+ \frac{3}{9} \langle \phi_1(11)11 | c_r^\dagger h c_r | \phi_1(11)11 \rangle \\ &+ \frac{5}{9} \langle \phi_1(11)21 | c_r^\dagger c_\Omega^\dagger h c_\Omega c_r | \phi_1(11)21 \rangle . \end{aligned} \quad (67)$$

As mentioned earlier, the long-range character of the tensor force leads to long-range tensor correlations. However, long-range tensor correlation functions are not desirable for several reasons: (i) The optimal long-range behavior would depend strongly on the nucleus under consideration. Hence, our goal of extracting the state-independent, universal correlations forbids long-range correlation functions. (ii) The two-body approximation would not be applicable for long-range correlators. (iii) Effectively, higher order contributions of the cluster expansion lead to a screening of long-range tensor correlations between two nucleons through the presence of other nucleons within the correlation range [16]. For these reasons, we constrain the range of the tensor correlation functions in our variational procedure. We use the following integral con-

T	I_ϑ [fm ³]	α [fm]	β [fm]	γ [fm]
0	0.03	491.32	0.9793	1000.0
0	0.04	521.60	1.0367	1000.0
0	0.05	539.86	1.0868	1000.0
0	0.06	542.79	1.1360	1000.0
0	0.07	543.21	1.1804	1000.0
0	0.08	541.29	1.2215	1000.0
0	0.09	536.67	1.2608	1000.0
0	0.10	531.03	1.2978	1000.0
0	0.11	524.46	1.3333	1000.0
0	0.12	517.40	1.3672	1000.0
1	0.01	-0.1036	1.5869	3.4426
1	0.02	-0.0815	1.9057	2.4204
1	0.03	-0.0569	2.1874	1.4761
1	0.04	-0.0528	2.3876	1.2610
1	0.05	-0.0463	2.6004	0.9983
1	0.06	-0.0420	2.7984	0.8141
1	0.07	-0.0389	2.9840	0.6643
1	0.08	-0.0377	3.1414	0.6115
1	0.09	-0.0364	3.2925	0.5473
1	0.10	-0.0353	3.4349	0.4997

TABLE II: Parameters of the tensor correlation functions $\vartheta(r)$ for the AV18 potential with different values I_ϑ for the range constraint obtained from two-body energy minimization.

straint on the “volume” of the tensor correlation functions

$$I_\vartheta = \int dr r^2 \vartheta(r). \quad (68)$$

The constrained energy minimization for the $S = 1, T = 0$ and the $S = 1, T = 1$ channels with different values of the tensor correlation volume I_ϑ leads to optimal parameters reported in Table II. The optimal parameters for the central correlation functions change only marginally with the tensor constraint. Therefore, we adopt a fixed set of parameters for the central correlators given in Table I.

The optimal central correlation functions for the AV18 potential are depicted in Fig. 2. In the even channels, the correlation functions decrease rapidly and vanish beyond $r \approx 1.5$ fm. The central correlators in the odd channels are weaker and of slightly longer range due to the influence of the centrifugal barrier. For the tensor correlation functions the constraints on the range are important. Fig. 3 shows the triplet-even (a) and triplet-odd (b) tensor correlation functions $\vartheta(r)$ for different I_ϑ . Because the tensor interaction is significantly weaker for $T = 1$ than for $T = 0$, the tensor correlator for this channel has a much smaller amplitude. The relevant values for the constraint I_ϑ are therefore smaller for the triple-odd channel.

We stress that the range constraint for the tensor correlation functions has an important physical and conceptual background. The Unitary Correlation Operator Method is used to describe state-independent short-range correlations only. Long-range correlations of any kind have to be described by

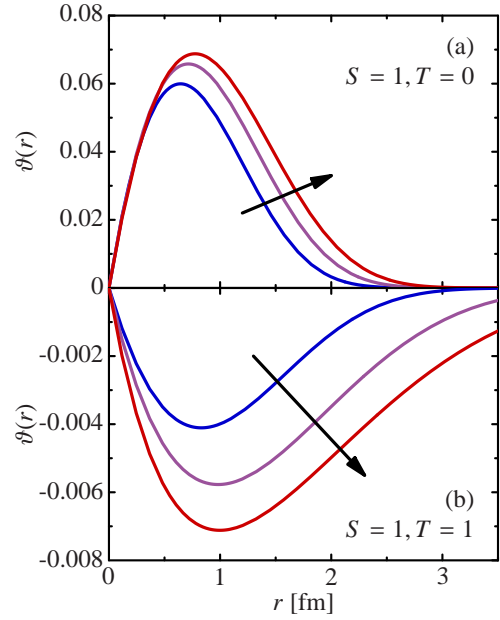


FIG. 3: (Color online) Optimal tensor correlation functions $\vartheta(r)$ for different values of the range constraint I_ϑ . (a) Correlation functions for $T = 0$ with $I_\vartheta = 0.06, 0.09,$ and 0.12 fm³. (b) Correlation functions for $T = 1$ with $I_\vartheta = 0.01, 0.03,$ and 0.06 fm³. The arrows indicate the direction of increasing I_ϑ .

the model space employed in the solution of the many-body problem. By constraining the range of the tensor correlators we set the separation scale between short-range and long-range correlations. The optimal value for tensor constraints cannot be fixed in the two-body system alone, but requires input from few-nucleon systems. We will come back to this point in Sec. VI.

V. PROPERTIES OF CORRELATED MOMENTUM-SPACE MATRIX ELEMENTS

A. Effect of the Correlators

In order to illustrate the effect of the unitary transformation in more detail, we discuss relative momentum space matrix elements of the form $\langle q(LS)JT | v_{\text{UCOM}} | q'(L'S)JT \rangle$, where q is the relative two-body momentum. The calculation of correlated momentum-space matrix elements is performed using the relations derived in Sec. III with radial wave functions given by the spherical Bessel functions.

First, we consider the full set of matrix elements in the (q, q') -plane for the lowest partial waves and compare the bare AV18 potential with the correlated interaction. The plots in Fig. 4 depict the matrix elements for the 1S_0 and 3S_1 partial waves as well as for the mixed $^3S_1 - ^3D_1$ channel (from top to bottom). The left-hand column corresponds to matrix elements of the bare AV18 potential, the center column to correlated matrix elements using the central correlator only, and the right-hand column to the fully correlated matrix elements of v_{UCOM} including central and tensor correlators.

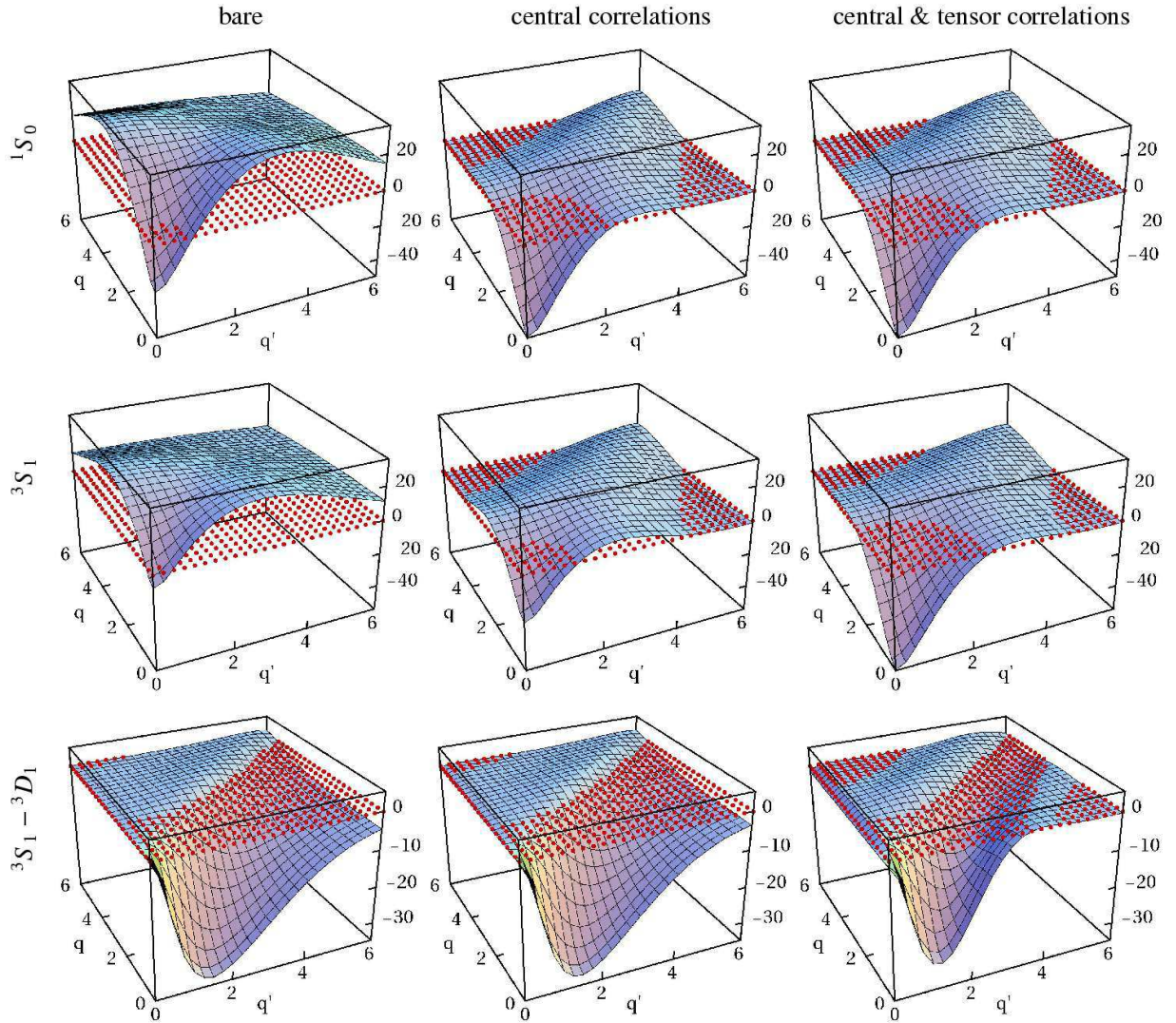


FIG. 4: (Color online) Relative momentum-space matrix elements of the bare AV18 potential (left-hand column), the central correlated AV18 potential (center column), and the fully correlated AV18 potential. The different rows correspond to different partial waves: 1S_0 (top row), 3S_1 (middle row), and $^3S_1 - ^3D_1$ (bottom row). The optimal tensor correlator for $I_\vartheta = 0.09 \text{ fm}^3$ is used. The red dots mark the plane of vanishing matrix elements. The momenta are given in units of $[\text{fm}^{-1}]$ and the matrix elements in $[\text{MeV}]$.

The gross effect of the unitary transformation on the dominant S -wave matrix elements depicted in the upper two rows of Fig. 4 is similar. In both cases the matrix elements of the bare interaction are predominantly repulsive except for a very small region at small momenta. The inclusion of the central correlator, accounting for correlations induced by the repulsive core of the interaction, causes a substantial change in the correlated matrix elements. In a region of low momenta $q, q' \lesssim 2 \text{ fm}^{-1}$ the matrix elements become strongly attractive. For larger momenta the magnitude of the matrix elements is reduced, outside a band along the diagonal the momentum space matrix elements practically vanish. Only within this band a moderate repulsion remains. The inclusion of the tensor correlator does not change the matrix elements in the spin-singlet channel. In the spin-triplet channel the addition of tensor correlations enhances the effect of the central correlations.

The attractive matrix elements at low momenta are enhanced while the off-diagonal matrix elements are further suppressed.

These matrix elements demonstrate the two major effects of the unitary correlators: (i) For the important $L = 0$ partial waves, the low-momentum matrix elements become strongly attractive as a result of the proper treatment of the correlations induced by the repulsive core and the tensor part. (ii) The off-diagonal matrix elements outside a band along the diagonal are strongly suppressed. Hence the unitary transformation acts like a *pre-diagonalization*.

The importance of tensor correlations is accentuated in the $^3S_1 - ^3D_1$ channel depicted in the bottom row of Fig. 4. For the bare interaction only the tensor part contributes to this channel and the matrix elements reveal strong off-diagonal contributions. In many-body calculations, e.g. in a shell-model framework, these off-diagonal matrix elements are re-

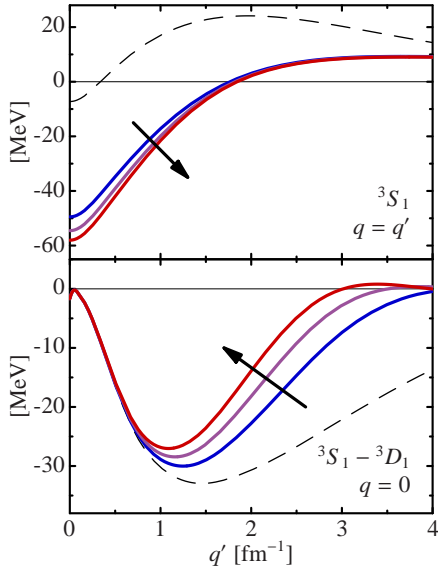


FIG. 5: (Color online) Momentum-space matrix elements of the correlated AV18 potential for different ranges of the tensor correlator (solid lines): $I_\vartheta = 0.06 \text{ fm}^3$, 0.09 fm^3 , 0.12 fm^3 . The arrow indicates the direction of increasing correlator range. The dashed line represents the matrix elements of the bare potential. The upper panel shows diagonal matrix elements in the 3S_1 channel as function of $q = q'$. The lower panel depicts the off-diagonal ${}^3S_1 - {}^3D_1$ matrix elements for fixed $q = 0$ as function of q' .

sponsible for the admixture of high-lying basis states to the ground state contributing strongly to the binding energy [27]. The effect of the central correlator on these matrix elements is marginal. The tensor correlator, however, causes a significant reduction of the off-diagonal matrix elements. Outside of a band along the diagonal the matrix elements vanish, i.e. the admixture of higher momenta or oscillator shells is suppressed significantly.

The off-diagonal contributions from the tensor interaction are not fully suppressed by the tensor correlators — only the high-momentum components are eliminated. This corresponds to the short-range part of the tensor correlations in coordinate space, which we constrained the tensor correlation operator to.

The dependence of the momentum space matrix elements on the range of the tensor correlation functions is illustrated in Fig. 5. Note that only the tensor correlation functions are changed, the central correlators stay the same. Therefore, only the matrix elements in the spin-triplet channels change, and of those the $S = 1$, $T = 0$ channels are affected most. The upper panel depicts the diagonal $q = q'$ matrix elements for the 3S_1 channel. With increasing correlator range I_ϑ , as indicated by the arrow, the attraction at low momenta is enhanced. This can be easily understood in the picture of correlated states: Longer-ranged tensor correlators generate a longer-range D -wave admixture such that the tensor attraction of the bare potential can be exploited to a larger degree. In the picture of a correlated Hamiltonian, the increased low-momentum attrac-

tion results from a transformation of longer-ranged components of the tensor interaction into operator channels which are accessible to uncorrelated S -wave states (cf. Sec. II F).

The off-diagonal matrix elements in the ${}^3S_1 - {}^3D_1$ channel show a complementary behavior. The lower panel in Fig. 5 depicts the off-diagonal matrix elements as functions of q' for fixed $q = 0$. As mentioned earlier, the matrix elements far off the diagonal are strongly suppressed by the unitary transformation—they are associated with short-range tensor correlations. With increasing range of the tensor correlator, off-diagonal matrix elements at successively lower momenta are suppressed as well. Hence the band of non-vanishing matrix elements along the diagonal is narrowed with increasing correlator range.

B. Comparison with $V_{\text{low}k}$

On the level of momentum-space matrix elements we can directly compare the correlated interaction v_{UCOM} with the $V_{\text{low}k}$ matrix elements resulting from a renormalization group decimation of the bare interaction [12, 13]. Both approaches aim at the construction of a phase-shift equivalent low-momentum interaction, though their formal background is completely different. The $V_{\text{low}k}$ approach relies on a decoupling of a low-momentum P -space, constrained by a momentum cutoff Λ , and a complementary high-momentum Q -space via a similarity transformation. After a second transformation in order to restore hermiticity, the momentum-space matrix elements within the P -space are obtained. Matrix elements between P and Q -space vanish by virtue of the decoupling condition, Q -space matrix elements are discarded (hence violating unitarity) such that nonvanishing matrix elements exist only for momenta below the cutoff. In contrast to v_{UCOM} the $V_{\text{low}k}$ approach is entirely formulated at the level of momentum-space matrix elements for the different partial waves. This entails that a general operator representation of the effective interaction is not directly accessible.

Despite their formal differences the matrix elements of both methods show a remarkable agreement in the dominant partial waves. Fig. 6 compares the $V_{\text{low}k}$ matrix elements for a cutoff momentum $\Lambda = 2.1 \text{ fm}^{-1}$ with the momentum-space matrix elements of v_{UCOM} obtained with the optimal correlators for $I_\vartheta = 0.08 \text{ fm}^3$. Up to momenta $q \approx 1.5 \text{ fm}^{-1}$ the matrix elements agree very well in most partial waves. For the dominant S -wave channels the agreement extends right up to the cutoff momentum for $V_{\text{low}k}$. Above the cutoff momentum the $V_{\text{low}k}$ matrix elements are zero by construction. In contrast, the matrix elements of v_{UCOM} continuously extend to larger momenta. This reflects the different conceptual ideas: Whereas $V_{\text{low}k}$ attempts a decimation of the interaction to low-momentum contributions below the cutoff scale, v_{UCOM} uses a prediagonalization of the matrix-elements by a unitary transformation.

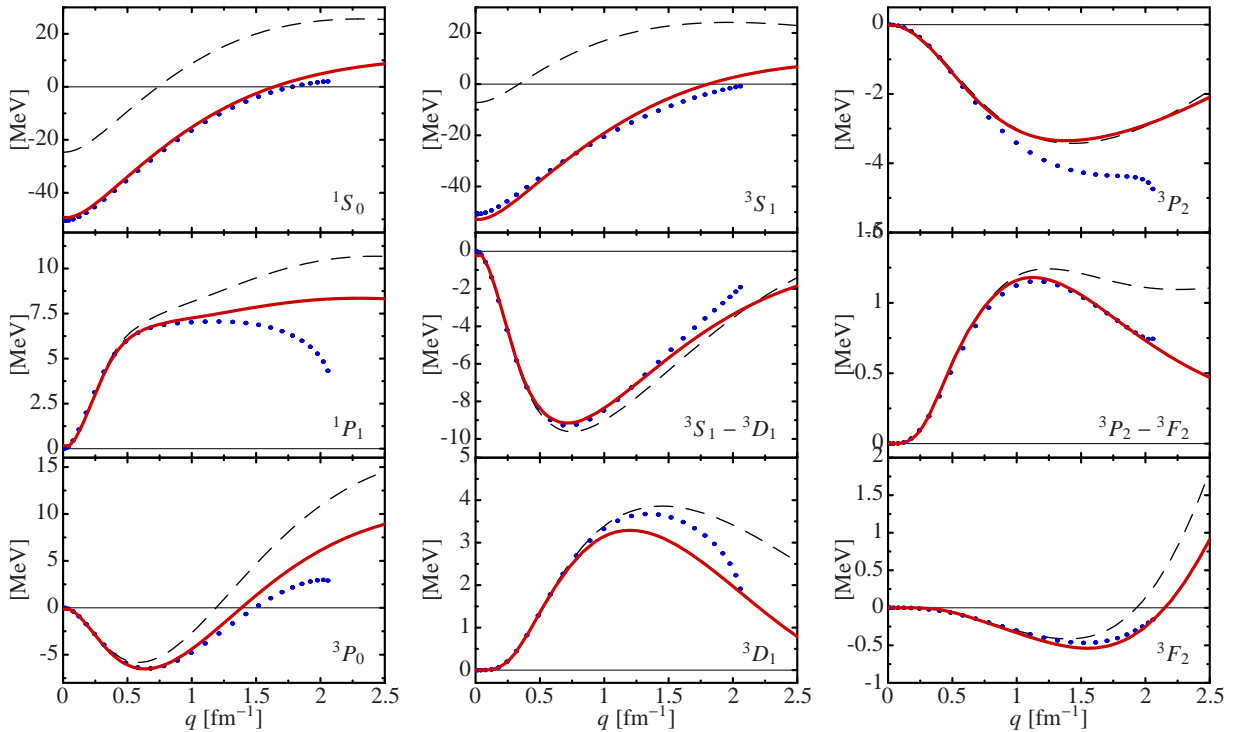


FIG. 6: (Color online) Comparison of the diagonal momentum space matrix elements of the correlated interaction v_{UCOM} (red lines) with the V_{lowk} matrix elements (blue dots) for the AV18 potential. The dashed line corresponds to the matrix elements of the bare potential. The optimal tensor correlators for $I_\vartheta = 0.08 \text{ fm}^3$ are used and the V_{lowk} momentum cutoff is $\Lambda = 2.1 \text{ fm}^{-1}$.

VI. FEW-BODY SHELL-MODEL CALCULATIONS

The correlated interaction and the correlated matrix elements can be used as input for all kinds of many-body calculations. We have already discussed nuclear structure studies in the framework of Fermionic Molecular Dynamics [15, 16], which rely on the operator form of the correlated interaction. The correlated matrix elements serve as an input for shell-model or Hartree-Fock calculations. In a forthcoming publication we will present nuclear structure calculations based on correlated realistic interactions in the framework of the Hartree-Fock and the Random Phase Approximation covering all mass regimes.

In this section we discuss the application of the correlated matrix elements in no-core shell model calculations for ${}^3\text{H}$ and ${}^4\text{He}$. These few-body systems provide important information on the correlated interaction beyond the two-body level. We use the no-core shell model code developed by Petr Navrátil et al. [28]. It is formulated in a translationally invariant harmonic oscillator basis using Jacobi coordinates. Input for the shell-model diagonalization are the relative two-body matrix elements of the correlated AV18 potential, including charge dependent terms and Coulomb interaction. We stress that the Lee-Suzuki transformation usually employed in the no-core shell-model [7, 9, 28] is not used here. We only perform a plain shell-model diagonalization. The task of transforming the bare interaction into an effective interaction suitable for shell-model calculations in small model-spaces is per-

formed by the unitary correlation operators.

The effect of the unitary correlation operators in a no-core shell model calculation for the ground state of ${}^4\text{He}$ is illustrated in Fig. 7. For a given size of the model-space, characterized by the maximum relative oscillator quantum number $\mathcal{N}_{\text{max}} = 2N_{\text{max}} + L_{\text{max}}$, the ground state energy is plotted as a function of the oscillator parameter $\hbar\Omega$. The upper panel depicts the shell-model result for the bare AV18 potential without any explicit treatment of correlations. All correlations induced by the interaction have to be described by the degrees of freedom of the model space alone. As expected, huge model spaces are required in order to adequately describe short-range correlations. Within the computational limits of $\mathcal{N}_{\text{max}} \leq 16$ for ${}^4\text{He}$, one is not able to achieve convergence with the bare interaction. The exact ${}^4\text{He}$ ground state energy for the AV18 potential [29] (marked by the horizontal line) is still somewhat lower than the result from the shell-model diagonalization for $\mathcal{N}_{\text{max}} = 16$.

The convergence behavior changes dramatically once we use the correlated matrix elements instead of the bare ones. The lower panel in Fig. 7 depicts the no-core shell model results for ${}^4\text{He}$ obtained with the correlated AV18 potential using the tensor correlator for $I_\vartheta = 0.09 \text{ fm}^3$ in the dominant $S = 1, T = 0$ channel. The $S = 1, T = 1$ channel is irrelevant for the nuclei considered in this section and the corresponding tensor correlation function is set to zero. The comparison with the calculation for the bare AV18 potential reveals three major effects of the unitary transformation:

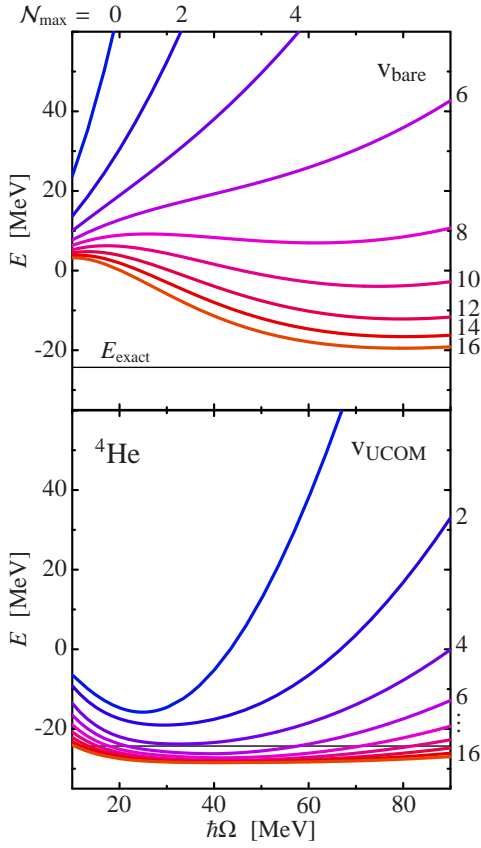


FIG. 7: (Color online) Ground state energy of ${}^4\text{He}$ as function of the oscillator parameter $\hbar\Omega$ for different model-space sizes $\mathcal{N}_{\text{max}} = 0, 2, \dots, 16$ as indicated by the labels. The upper panel shows results for the bare AV18 potential, the lower panel corresponds to the correlated potential v_{UCOM} for $I_\theta = 0.09 \text{ fm}^3$. The horizontal lines represent the exact binding energy for the bare potential taken from [29].

(i) The ground state energy for very small model spaces, e.g. $\mathcal{N}_{\text{max}} = 0$, for which the space consists of a single Slater determinant, is lowered dramatically. Evidently, the inclusion of the dominant short-range central and tensor correlations through the unitary transformation is sufficient to reproduce the bulk of the binding energy.

(ii) With increasing model-space size the energy is lowered by a moderate amount. The convergence is drastically improved. Fully converged results, featuring a flat energy curve over a significant range of oscillator parameters $\hbar\Omega$ can be obtained in spaces of moderate size. The energy gain compared to the results in small model-spaces can be attributed to residual *long-range* correlations not described by the unitary correlator. In contrast to *short-range* correlations, these *long-range* correlations can be described quite easily in model-spaces of manageable size, hence the fast convergence.

(iii) The converged energy is generally below the exact ground state energy for the potential under consideration. This violation of the variational bound is solely due to the omission of the three- and four-body terms in the cluster expansion (17)

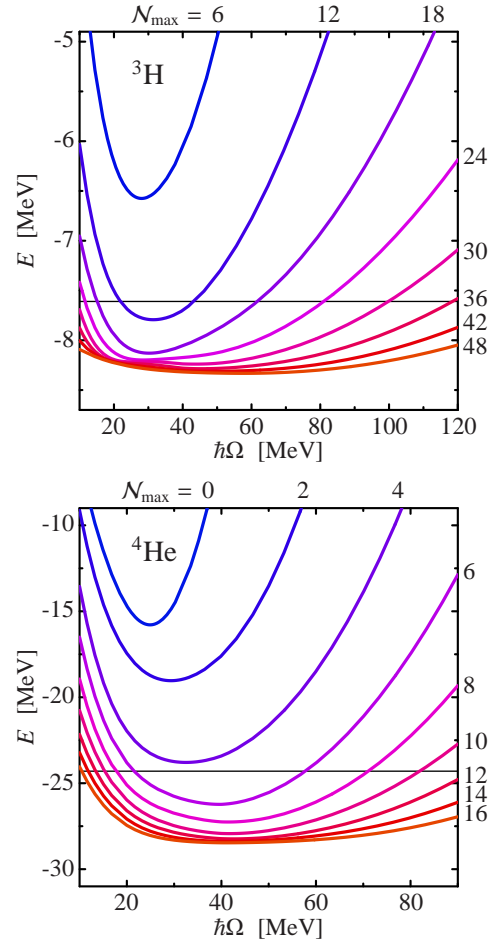


FIG. 8: (Color online) Ground state energy of ${}^3\text{H}$ and ${}^4\text{He}$ as function of the oscillator parameter $\hbar\Omega$ for the correlated AV18 potential ($I_\theta = 0.09 \text{ fm}^3$) obtained in a no-core shell-model diagonalization. The different curves correspond to different model-space sizes \mathcal{N}_{max} as indicated by the labels. The horizontal lines represent the exact binding energies for the bare potential taken from [29].

of the correlated Hamiltonian. As a direct consequence of the unitarity of the transformation, the exact energy eigenvalues of the correlated Hamiltonian including all terms of the cluster expansion are identical to the exact energy eigenvalues of the bare Hamiltonian. Hence, the difference between the exact result using the bare interaction and the correlated interaction in two-body approximation equals the contribution of higher cluster orders and thus provides a quantitative measure for the quality of the two-body approximation.

A more detailed view of the convergence behavior for the correlated AV18 potential is presented in Fig. 8 for ${}^3\text{H}$ and ${}^4\text{He}$. For both systems the three aforementioned effects can be observed. The convergence for ${}^3\text{H}$ is somewhat slower because of the long-range structure of the wave function which cannot easily be described within the oscillator basis.

The no-core shell model results directly reflect the basic aims of the Unitary Correlation Operator Method. The short-range correlations are described explicitly by a state-

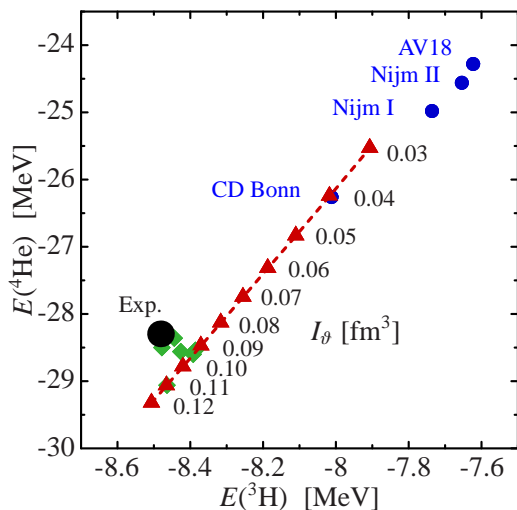


FIG. 9: (Color online) Binding energies of ${}^4\text{He}$ versus ${}^3\text{H}$. The blue discs show the results of exact Faddeev calculations obtained by A. Nogga et al. [29] using different modern NN-potentials. The green diamonds show results obtained by including simple three-body forces in addition to the realistic two-nucleon potentials [29]. The red triangles are the converged no-core shell model results for the correlated AV18 potential for different values $I_\vartheta = 0.03, \dots, 0.12 \text{ fm}^3$ of the range-constraint for the tensor correlator.

independent unitary transformation such that the bulk of the binding energy can readily be obtained in very small model spaces. Residual system-dependent long-range correlations have to be described by the model space, which is easily possible in the framework of the no-core shell model.

Considering the omission of the higher-order terms in the cluster expansions, the no-core shell model results allow for a study of the range-dependence of these contributions. The difference between converged result and exact calculations with the bare potential, i.e., the size of the omitted three- and four-body terms, increases with increasing range of the tensor correlators. This dependence is summarized in Fig. 9, where we plot the ground state energies of ${}^4\text{He}$ and ${}^3\text{H}$ in the $E({}^3\text{H})-E({}^4\text{He})$ plane. The results for different tensor correlators with range constraints $I_\vartheta = 0.03, \dots, 0.12 \text{ fm}^3$ (cf. Tab. II) are represented by the triangles. All those points fall onto a straight line. Moreover, this line coincides with the so-called Tjon-line [29], which characterizes a correlation between the ${}^4\text{He}$ and ${}^3\text{H}$ binding energies found for different realistic two-body potentials that reproduce the same phase shifts (blue discs in Fig. 9). It is not surprising that the correlated interactions follow the same trend, because the correlated interaction v_{UCOM} generates the same phase-shifts as the original potential. For each set of correlators, the resulting correlated interaction v_{UCOM} provides a new phase-shift equivalent realistic potential. The value of the range constraint I_ϑ can be used to map out the Tjon line. A similar behavior was observed for the V_{lowk} interaction as a function of the cutoff parameters [30].

In our calculation only the range of the tensor correlators

in the spin-triplet channels is varied and of those only the $S = 1, T = 0$ channel is relevant for ${}^4\text{He}$ and ${}^3\text{H}$. Hence, the variation along the Tjon-line is related exclusively to the tensor correlations. As discussed in Sec. II E, the unitary transformation of the Hamiltonian with the tensor correlators produces additional momentum-dependent tensor terms in v_{UCOM} as well as different central contributions. The non-local tensor contributions seem to play an important role regarding the Tjon-line: Increasing the strength of the non-local tensor contribution by increasing the strength of the tensor correlators shifts the binding energies towards the experimental values and away from the realistic potentials with purely local tensor contributions. This is in accord with the results for the CD Bonn potential, which is the only one among the high-precision NN-potentials including non-local tensor contributions [26].

By choosing an appropriate value for the range constraint, one obtains a phase-shift equivalent two-body potential, which produces binding energies for ${}^4\text{He}$ and ${}^3\text{H}$ close to the experimental point (cf. Fig. 9). This is the result of a subtle cancellation between different three-body contributions. For exact calculations using the bare potentials one immediately finds that the two-body potential alone (blue discs in Fig. 9) does not generate enough binding. It has to be supplemented by a three-body force which produces a net attraction. The green diamonds in Fig. 9 show results obtained by A. Nogga et al. [29] using various simple parametrizations of phenomenological three-nucleon forces supplementing the different realistic two-body potentials. For the calculation with the correlated interactions we have not included any of the three-body contributions, i.e., neither the genuine three-body force nor the three-body contributions of the cluster expansion are taken into account. The proximity to the experimental point for, e.g. $I_\vartheta = 0.09 \text{ fm}^3$, thus indicates, that the omitted three-body terms of the cluster expansion can be tuned such that they cancel the contributions of the genuine three-body force to a large extent. The influence of the genuine three-body force on the binding energies in these small systems can therefore be minimized by a proper choice of the correlators, i.e., by choosing the phase-shift equivalent two-body force which needs the weakest three-body force. This, however, does not mean that the three-body force can be avoided completely. One should keep in mind that the above observations refer to a single observable and to very small systems only.

VII. CONCLUSIONS

The Unitary Correlation Operator Method provides a powerful and transparent tool to construct phase-shift equivalent low-momentum interactions by means of an explicit unitary transformation of a realistic NN-potential. The physics of short-range central and tensor correlations is encapsulated in the optimal correlators which are determined in the two-body system. For the long-ranged tensor component a separation of short-range state-independent correlations and long-range correlations is performed through an additional constraint on

the range of the correlators. Once the correlators are fixed, we can evaluate the unitary transformation of either states or operators directly.

In the case of two-body matrix elements of the correlated Hamiltonian in an LS -coupled basis, it is convenient to map the unitary correlators onto the two-body angular momentum eigenstates. The resulting correlated matrix elements reveal some of the important features of the correlated interaction. The unitary transformation causes a pre-diagonalization of the Hamiltonian, i.e., large off-diagonal momentum-space matrix elements induced by the central core and the tensor interaction are eliminated and non-vanishing matrix elements remain solely in a band along the diagonal.

Correlated matrix elements, e.g. with respect to a harmonic oscillator basis, serve as universal input for different many-body calculations [32]. We have demonstrated the use of those matrix elements in the no-core shell model for $A \leq 4$. In comparison to a shell-model diagonalization with the bare interaction we observe a dramatic reduction of the ground state energy in very small model-spaces and a significant improvement of convergence with increasing size of the model space. Here the interplay between unitary correlator and model-space becomes evident: The unitary correlation operator describes the state-independent short-range correlations induced by the central and the tensor part of the interaction — this accounts for the bulk of the binding energy. State-dependent long-range correlations are described by the model-space — this leads to the moderate gain in binding energy with increasing model

space size. The rapid convergence indicates that those long-range correlations, unlike the short-range correlations, can be quite easily treated in small and computationally accessible model-spaces.

The no-core shell model calculations also provide a guideline for the choice of the range-constraint for the tensor correlators. As function of the range of the tensor correlators a manifold of phase-shift equivalent potentials is generated which map out the Tjon line. The correlator range can be chosen such that the exact ground state energies for $A \leq 4$ are in good agreement with experiment. Thus the net impact of the residual three-nucleon force on the binding energies in these small systems can be minimized.

The next step is to use the correlated matrix elements as input for nuclear structure calculations also for heavier isotopes. In a forthcoming publication we will discuss Hartree-Fock as well as RPA calculations across the whole nuclear chart using the same correlated realistic interactions.

Acknowledgments

We are very grateful to Petr Navrátil for providing us with the no-core shell model code used in Sec. VI. We thank Achim Schwenk for the V_{lowk} matrix elements used in Fig. 6. This work is supported by the Deutsche Forschungsgemeinschaft through contract SFB 634.

-
- [1] R. B. Wiringa, V. G. J. Stoks, and R. Schiavilla, Phys. Rev. C **51**, 38 (1995).
 - [2] R. Machleidt, Phys. Rev. C **63**, 024001 (2001).
 - [3] V. G. J. Stoks, R. A. M. Klomp, C. P. F. Terheggen, and J. J. de Swart, Phys. Rev. C **49**, 2950 (1994).
 - [4] S. C. Pieper, K. Varga, and R. B. Wiringa, Phys. Rev. C **66**, 044310 (2002).
 - [5] S. C. Pieper and R. B. Wiringa, Ann. Rev. Nucl. Part. Sci. **51**, 53 (2001).
 - [6] S. C. Pieper, R. B. Wiringa, and J. Carlson, Phys. Rev. C **70**, 054325 (2004).
 - [7] E. Caurier, P. Navrátil, W. E. Ormand, and J. P. Vary, Phys. Rev. C **66**, 024314 (2002).
 - [8] P. Navrátil and W. E. Ormand, Phys. Rev. Lett. **88**, 152502 (2002).
 - [9] P. Navrátil, J. P. Vary, and B. R. Barrett, Phys. Rev. C **62**, 054311 (2000).
 - [10] D. R. Entem and R. Machleidt, Phys. Rev. C **68**, 041001(R) (2003).
 - [11] E. Epelbaum, A. Nogga, W. Glöckle, H. Kamada, Ulf-G. Meißner, and H. Witala, Phys. Rev. C **66**, 064001 (2002).
 - [12] S. K. Bogner, T. T. S. Kuo, and A. Schwenk, Phys. Rep. **386**, 1 (2003).
 - [13] S. K. Bogner, T. T. S. Kuo, A. Schwenk, D. R. Entem, and R. Machleidt, Phys. Lett. B **576**, 265 (2003).
 - [14] H. Feldmeier, T. Neff, R. Roth, and J. Schnack, Nucl. Phys. **A632**, 61 (1998).
 - [15] T. Neff and H. Feldmeier, Nucl. Phys. **A713**, 311 (2003).
 - [16] R. Roth, T. Neff, H. Hergert, and H. Feldmeier, Nucl. Phys. A **745**, 3 (2004).
 - [17] T. Neff and H. Feldmeier, Nucl. Phys. A **738**, 357 (2004).
 - [18] T. Neff, H. Feldmeier, and R. Roth, Nucl. Phys. A **752**, 321 (2005).
 - [19] K. Suzuki and S. Y. Lee, Prog. Theo. Phys. **64**, 2091 (1980).
 - [20] S. Fujii, R. Okamoto, and K. Suzuki, Phys. Rev. C **69**, 034328 (2004).
 - [21] R. Roth, Ph.D. thesis, Technische Universität Darmstadt (2000).
 - [22] R. Machleidt, Adv. Nucl. Phys. **19**, 189 (1989).
 - [23] H. Feldmeier, Nucl. Phys. **A515**, 147 (1990).
 - [24] H. Feldmeier and J. Schnack, Rev. Mod. Phys. **72**, 655 (2000).
 - [25] I. Stetcu, B. R. Barrett, P. Navrátil, and J. P. Vary, Phys. Rev. C **71**, 044325 (2005).
 - [26] R. Machleidt and I. Slaus, J. Phys. G: Nucl. Part. Phys. **27**, R69 (2001).
 - [27] J. P. Vary, P. U. Sauer, and C. W. Wong, Phys. Rev. C **7**, 1776 (1973).
 - [28] P. Navrátil, G. P. Kamuntavicius, and B. R. Barrett, Phys. Rev. C **61**, 044001 (2000).
 - [29] A. Nogga, H. Kamada, and W. Glöckle, Phys. Rev. Lett. **85**, 944 (2000).
 - [30] A. Nogga, S. K. Bogner, and A. Schwenk, Phys. Rev. C **70**, 061002(R) (2004).
 - [31] Small (capital) letters are used for correlation operators in two-body (A -body) space.
 - [32] An optimized code for the calculation of the correlated oscillator matrix elements is available from the authors upon request.